PIECEWISE-DIFFEOMORPHIC REGISTRATION OF 3D CT/MR PULMONARY IMAGES WITH SLIDING CONDITIONS

Laurent Risser[1], *Mattias P. Heinrich*[1], *Tahreema Matin*[2], *Julia A. Schnabel*[1]

[1]Institute of Biomedical Engineering, Department of Engineering Science, University of Oxford, UK
[2]Department of Radiology, Churchill Hospital, Oxford, UK

ABSTRACT

In this paper, we present a new algorithm to register 3D multi-modal images with sliding conditions in a diffeomorphic framework. Our driving motivation is to define one-to-one mappings between CT/MR pulmonary volumes acquired from patients with empyema. The main problem to overcome is that the pulmonary motion, which can be large, presents sliding conditions at the thoracic cage boundary. Our algorithm is therefore piecewise-diffeomorphic as it ensures the definition of one-to-one mappings with discontinuous deformations at the location of the sliding conditions. Its performance is demonstrated on 14 CT/MR image volumes of the chest. Results show that the estimated deformations are similar to those obtained using free-form deformations, with the additional property to ensure the invertibility of the deformations and to explicitly model the sliding motion at the thoracic cage boundary.

Index Terms— Diffeomorphic registration, sliding motion, multi-modal registration, lung motion correction

1. INTRODUCTION

The driving motivation of our work is to define one-to-one mappings between CT/MR 3D pulmonary images acquired from patients with empyema, as illustrated in Fig. 1. This disease is an infection of the lung pleura which leads to an excess fluid to fill up the pleural space (pleural effusion), which can cause the lungs to collapse. CT and MR images are useful to detect empyema but, for each patient, they may be scanned at different levels of breath-hold. A non-rigid alignment of both modalities has therefore a great potential to support the diagnostic task. This task is difficult to solve by using standard 3D registration algorithms for three reasons: (1) Sliding conditions occur at the thoracic cage boundaries, (2) the CT images have typically a resolution of about $0.6\times0.6\times2.5\text{mm}^3$ but the MR images may have a slice thickness of up to 10 mm for a typical planar resolution of $1.5\times1.5\text{mm}^2$ and (3) the CT/MR images contain sparsely distributed features to register. The issues 2 and 3 suggest that the registration should be performed with a large amount of regularisation. This is compatible with the smooth deformations observed within the lungs. This is however critical for capturing the sliding motion at their boundary. In addition, the relatively large amplitude of the respiratory motion can make the estimation of one-to-one mappings between the CT and MR images by using non-diffeomorphic registration techniques difficult. In this paper, we therefore propose an algorithm to perform diffeomorphic multi-modal image registration with the incorporation of sliding constraints.

LR and JAS acknowledge fundings from EPSRC EP/H050892/1 and the Cancer Research UK / EPSRC Oxford Cancer Imaging Centre (OCIC). MPH is funded by OCIC. Corresponding author: laurent.risser@gmail.com .

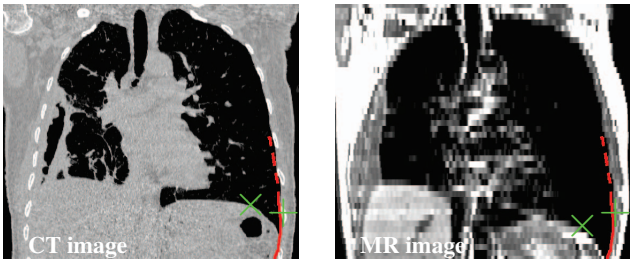


Fig. 1. Two registered 3D CT/MR images. Sliding conditions may occur at the thoracic cage boundary (*e.g.* red curve). The crosses $+$ and $\times$ respectively show a rib and a point at the boundary between the lungs and the diaphragm. Although $+$ nearly remains at the same location, $\times$ clearly moves down with the rest of the boundary. The sliding motion is obvious here.

A comparison of state-of-the art techniques for the registration of the lungs in CT images, without sliding conditions, has been recently published in [1]. More exploratory papers [2–7] introduced strategies for direction-dependent regularisation in diffusion-based registration frameworks. Though promising to capture the sliding motion between two images, these methods cannot ensure the deformations invertibility as the motion is encoded in displacement fields. We proposed the first diffeomorphic approach using time-dependent velocity fields to capture sliding conditions [8]. This approach however does not constrain the temporal smoothness of the deformations and requires too much memory to register large 3D images. In this paper, our key contribution is to propose a new extension of the Log-Demons framework [9] making possible the estimation of a sliding motion. This extension makes use of stationary velocity fields as in [9]. It therefore enables the registration of 3D images with reasonable computational resources and does not require any temporal regularisation of the deformations. It also ensures the definition of one-to-one mappings. The above mentioned techniques are limited to the registration of images of the same modality. Several techniques have been proposed to estimate local gradients of mutual information (MI) in demon-like algorithms [10–12]. Here, we propose to combine our sliding motion strategy with the MI-based demon forces of [12].

The paper is organised as follows. After presenting the Log-Demons formalism [9], we propose its piecewise-diffeomorphic extension which can incorporate sliding conditions. We then explain how we estimate multi-modal demon forces. We finally present results obtained for 3D synthetic CT/CT pulmonary images and 3D CT/MR pulmonary images of patients with empyema.

2. PIECEWISE-DIFFEOMORPHIC IMAGE REGISTRATION WITH SLIDING CONDITIONS

2.1. Overview of the Log-Demons formalism

Let I_S be a source image registered on a target image $I_T \in \Omega$. The image I_S is transformed through the time-dependent diffeomorphic transformation $\phi_{\mathbf{t}}^{\mathbf{v}}$, $t \in [0,1]$ which is defined by a stationary velocity field $\mathbf{v} \in \Omega$ using: $\frac{\partial}{\partial_t}\phi_{\mathbf{t}}^{\mathbf{v}} = \mathbf{v}(\phi_{\mathbf{t}}^{\mathbf{v}})$, where $\phi_{\mathbf{0}}^{\mathbf{v}} = \mathbf{Id}$. The optimal velocity field $\tilde{\mathbf{v}}$ is obtained by minimising $\tilde{\mathbf{v}} = \arg\min_{\mathbf{v}} E(\mathbf{v}, \mathbf{v_c})$, where the energy E is defined as:

$$E(\mathbf{v}, \mathbf{v_c}) = \frac{1}{\lambda_i^2}||I_T - I_S \circ \phi_{\mathbf{1}}^{\mathbf{v_c}}||_{L^2}^2 + \frac{1}{\lambda_x^2}||\log((\phi_{\mathbf{1}}^{\mathbf{v}})^{-1} \circ \phi_{\mathbf{1}}^{\mathbf{v_c}})||_{L^2}^2 + \frac{1}{\lambda_d^2}||\nabla \mathbf{v}||_{L^2}^2 \quad (1)$$

where the logarithm $\log(\kappa)$ is the stationary velocity field encoding the deformation field κ, and $\mathbf{v_c}$ encodes an intermediate transformation $\phi_{\mathbf{1}}^{\mathbf{v_c}}$, called correspondence. In Eq. (1), the first term measures the sum of squared differences (SSD) between the registered image intensities, the second term measures the correspondence between the smooth deformation $\phi_{\mathbf{1}}^{\mathbf{v}}$ and the deformation $\phi_{\mathbf{1}}^{\mathbf{v_c}}$, and the third term measures the spatial regularity of $\mathbf{v}$. The influence of the parameters λ_i, λ_x, λ_d is developed in [9]. After initialising $\mathbf{v}$ and $\mathbf{v_c}$ as zero, $E(\mathbf{v}, \mathbf{v_c})$ is minimised iteratively: *(i)* An update velocity field $\delta\mathbf{v}$ is firstly computed using:

$$\delta\mathbf{v}(\mathbf{x}) = -\frac{I_T - I_S \circ \phi_{\mathbf{1}}^{\mathbf{v}}}{||\mathbf{J}(\mathbf{x})||^2 + \lambda_i^2/\lambda_x^2}\mathbf{J}(\mathbf{x}), \quad (2)$$

where the $\mathbf{J}(\mathbf{x}) = \nabla(I_S \circ \phi_{\mathbf{1}}^{\mathbf{v}})(\mathbf{x})$, $\mathbf{x} \in \Omega$, are the intensity gradients. *(ii)* The update field $\delta\mathbf{v}$ may be smoothed by a Gaussian kernel (fluid regularisation). *(iii)* Estimation of $\mathbf{v_c} = log(\phi_{\mathbf{1}}^{\mathbf{v}} \circ \phi_{\mathbf{1}}^{\delta\mathbf{v}})$ is addressed using the Baker-Campbell-Hausdorff (BCH) formula: $\mathbf{v_c} \simeq \mathbf{v} + \delta\mathbf{v} + [\mathbf{v}, \delta\mathbf{v}]/2$, where the Lie bracket $[.,.]$ is defined by $[\mathbf{v_1}, \mathbf{v_2}] = (\nabla\mathbf{v_1})\mathbf{v_2} - (\nabla\mathbf{v_2})\mathbf{v_1}$. *(iv)* Finally, $\mathbf{v}$ is updated by smoothing $\mathbf{v_c}$ using a Gaussian kernel (diffusion regularisation).

2.2. Piecewise-Diffeomorphic Log-Demons

In order to perform piecewise-diffeomorphic registration, we modify the smoothing steps of the Log-Demons algorithm. We subdivide the domain Ω into two regions: the thoracic cage Ω_T and the rest of the image Ω_R. Instead of smoothing $\delta\mathbf{v}$ and $\mathbf{v_c}$ homogeneously in space, we smooth them in Ω_T and in Ω_R independently. In what follows, we describe the smoothing of a general velocity field $\mathbf{w}$ in a region Ω_i. We diffuse $\mathbf{w}$ using the heat equation $\partial\mathbf{w}/\partial\tau = \nabla^2\mathbf{w}$ in Ω_i during the *virtual* time $\tau \in [0, \Gamma]$ and model Neumann conditions at the region boundaries $\partial\Omega_i$. In an infinite domain, it can be shown that diffusing $\mathbf{w}$ during $\tau \in [0, \Gamma]$ is equivalent to smoothing $\mathbf{w}$ with a Gaussian kernel of standard deviation $\sqrt{2\Gamma}$ (Weierstrass transform). Our smoothing therefore differs from a standard Gaussian convolution only in the neighbourhood of $\partial\Omega_i$, where no information is shared with the voxels outside of Ω_i. Note that our implementation of the heat equation does not have any Courant-Friedrichs-Lewy (CFL) condition as we use an implicit scheme.

Our strategy can capture sliding conditions in Ω_T and in Ω_R. As shown in Fig. 2, it may however estimate velocity fields $\mathbf{v}$ that are not parallel to the boundaries in the neighbourhood of $\partial\Omega_i$, which leads to non-natural deformations. We therefore post-treat the smoothing step of $\mathbf{v}$, as shown between (b) and (c) in Fig. 2. We consider a vector field $\mathbf{D}$ so that, for each point $\mathbf{x} \in \Omega$, $\mathbf{x} + \mathbf{D}(\mathbf{x})$ is the closest

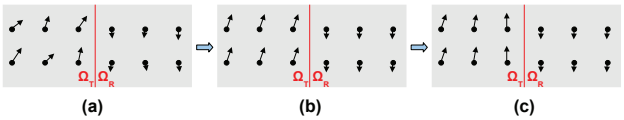


Fig. 2. Modified smoothing steps. **(a)** Initial velocity field $\delta\mathbf{v}$ or $\mathbf{v_c}$ in a small ROI. The red line represents the boundary between Ω_T and Ω_R. **(b)** Velocity field independently smoothed in Ω_T and in Ω_R. **(c)** Post-treatment to force the velocity field to be parallel to the region boundaries, close to the boundaries (only for $\mathbf{v}$).

boundary between Ω_T and Ω_R to $\mathbf{x}$. This field is constructed once for all prior to the image registration. We reduce the contributions of $\mathbf{v}(\mathbf{x})$ in the direction of $\mathbf{D}(\mathbf{x})$, when $||\mathbf{D}(\mathbf{x})|| < \gamma$ using:

$$\mathbf{v}(\mathbf{x}) \leftarrow \mathbf{v}(\mathbf{x}) - \alpha(\mathbf{x})\mathbf{D}(\mathbf{x})\frac{< \mathbf{v}(\mathbf{x}), \mathbf{D}(\mathbf{x}) >}{||\mathbf{D}(\mathbf{x})||^2}, \quad (3)$$

where $< .,. >$ stands for the scalar product. We compute $\alpha(\mathbf{x})$ using $(\gamma - ||\mathbf{D}(\mathbf{x})||)^2/\gamma$ and typically use a distance γ of 20 mm.

2.3. Multi-modal demon forces

We perform multi-modal registration by measuring the similarity between $I_S \circ \phi_{\mathbf{1}}^{\mathbf{v}}$ and I_T using the mutual information (MI) instead of the sum of squared differences (SSD) of [9]:

$$MI(\mathbf{v}) = -\sum_{i \in L_S}\sum_{j \in L_T} p(i,j;\mathbf{v}) \log_2\left(\frac{p(i,j;\mathbf{v})}{p_S(i;\mathbf{v})p_T(j)}\right), \quad (4)$$

where L_S and L_T are the discrete sets of intensities associated with $I_S \circ \phi_{\mathbf{1}}^{\mathbf{v}}$ and I_T. We build the Parzen windows using cubic B-splines as in [13]. The joint Parzen discrete probability between $I_S \circ \phi_{\mathbf{1}}^{\mathbf{v}}$ and I_T is then:

$$p(i,j;\mathbf{v}) = \frac{\alpha(\mathbf{v})}{\epsilon_S\epsilon_T}\sum_{\mathbf{x}\in\Omega}\omega_S\left(\frac{i - I_S \circ \phi_{\mathbf{1}}^{\mathbf{v}}(\mathbf{x})}{\epsilon_S}\right)\omega_T\left(\frac{j - I_T(\mathbf{x})}{\epsilon_T}\right), \quad (5)$$

where ϵ_T and ϵ_S are scaling factors controlling the size of the Parzen windows, $\alpha(\mathbf{v})$ is the normalizing constant of the probabilities and $p_S(i;\mathbf{v})$ and $p_T(j)$ are the marginal discrete probabilities. We estimate the multi-modal demon forces $\delta\mathbf{v}(\mathbf{x})$ proposed by [12] instead of those of Eq. (2):

$$\delta\mathbf{v}(\mathbf{x}) = \frac{\frac{\partial MI}{\partial \mu_{\mathbf{x}}}}{||\mathbf{J}(\mathbf{x})||^2 + \frac{||\frac{\partial MI}{\partial \mu_{\mathbf{x}}}||^2}{\sigma_x}}\mathbf{J}(\mathbf{x}). \quad (6)$$

In Eq. (6), the $\partial MI/\partial\mu_{\mathbf{x}}$ are estimated using an adaptive forward/backward finite differences strategy: $\partial MI/\partial\mu_{\mathbf{x}} \approx \min(S(\mathbf{x}^+) - S(\mathbf{x}), S(\mathbf{x}) - S(\mathbf{x}^-))/\delta$, where $S(\mathbf{x})$ comes from [13]:

$$S(\mathbf{x}) = \sum_{i \in L_S}\sum_{j \in L_T} I_S \circ \phi_{\mathbf{1}}^{\mathbf{v}}(\mathbf{x_n}) \left.\frac{\partial\omega_S(\xi)}{\partial\xi}\right|_{\xi = \frac{i - I_S \circ \phi_{\mathbf{1}}^{\mathbf{v}}(\mathbf{x_n})}{\epsilon_S}} \omega_T\left(\frac{j - I_T(\mathbf{x_n})}{\epsilon_T}\right)\log_2\left(\frac{p(i,j;\mu)}{p_S(i;\mu)}\right), \quad (7)$$

and $\mathbf{x}^+$ and $\mathbf{x}^-$ are equal to $\mathbf{x} \pm \delta\mathbf{J}(\mathbf{x})/||\mathbf{J}(\mathbf{x})||^2$.

3. RESULTS

First, we evaluate our contribution of incorporating sliding motion in the Log-Demons algorithm. For this, we apply our method to the registration of 3D phantom CT images. To evaluate the additional use of MI-based demon forces, we then register the real 3D multi-modal images presented in the introduction. In our tests, sliding conditions are modelled at the thoracic cage boundary. Thoracic cages were segmented by using template registration on the CT images and visual assessment. Our piecewise-diffeomorphic strategy also requires fixed subdomains Ω_T and Ω_R, although the thorax boundaries move during the respiratory cycle. This motion however tends to be very smooth. Standard Log-Demons registration with a large amount of regularisation was then performed as a first step to align the boundaries. It is worth mentioning that the discretisation of $\phi_{\mathbf{t}}^{\mathbf{v}} = \mathbf{v}(\phi_t^{\mathbf{v}})$ for $t \in [0,1]$ and the discontinuity at the boundary $\partial\Omega_T$ may lead to the estimation of some negative Jacobians there. This phenomenon is avoided by using fine temporal grids (128 time steps in our tests) and by smoothing the final velocity fields $\mathbf{v}$ using a fine Gaussian kernel (0.8 mm) in the neighbourhood of $\partial\Omega_T$.

Materials: The phantom dataset was generated using the 4D NURBS-based Cardiac-Torso (NCAT phantom) toolkit [14]. Two images of $96 \times 96 \times 96$ voxels representing the lungs at the end of expiration and at the end of inhalation were generated and registered with the standard Log-Demons algorithm of [9] and its piecewise-diffeomorphic extension, presented in subsection 2.2. We also registered 14 multi-modal CT/MR 3D images acquired on patients suffering from empyema, as presented in the introduction. For each patient, we rigidly aligned the images and defined a region of interest of about $300\times300\times70$ voxels in the target MR images. Multi-modal registration was performed using mutual-information Log-Demons with or without sliding motion modelling respectively. For comparison purposes, we also used the standard free-form deformation algorithm of [15][1] with default parameters.

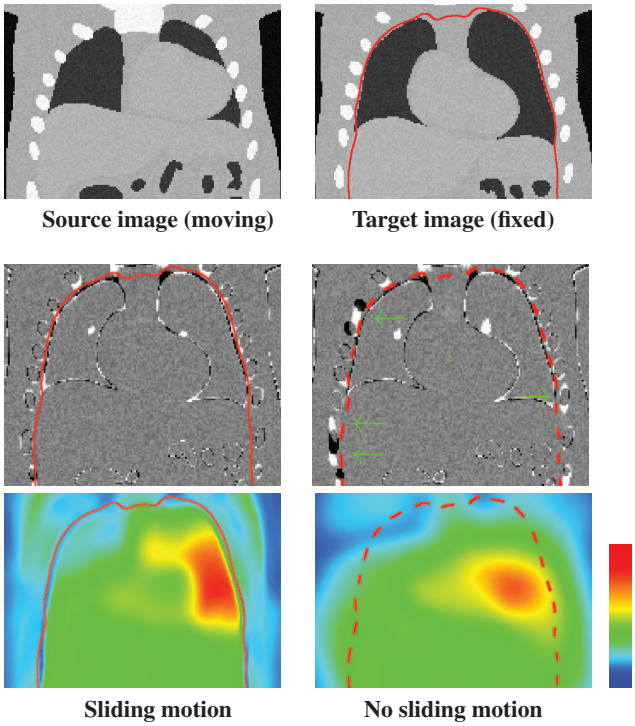


Fig. 3. Registration of two 3D phantom images with or without sliding conditions. The red line represents where the sliding motion is modelled. **(Row 2)** Difference between the registered images. **(Row 3)** Amplitude of the 3D deformations. Colour bar is from 0 to 30 mm.

NCAT images: Results obtained for the NCAT 3D images are illustrated in Fig. 3. The lungs' overlap (Dice's coefficients) between the registered images is 88% before registration and 97% after registration for both with or without sliding motion modelling respectively. More interestingly, the sliding conditions improve the matching accuracy of the ribs. This is emphasised by the arrows in the second row of Fig. 3. The ribs' overlap is 61% before registration, 79% after registration without sliding conditions and 86% after registration with sliding conditions. This becomes obvious when looking at the third row of Fig. 3: The general motion down of the thoracic cage (in green) is propagated outside of the cage by the regularisation when no sliding conditions are modelled.

CT/MR images: As shown in Fig. 4, the MI appears to converge when registering 4 typical CT/MR scans with sliding conditions. This is particularly important as the mathematical relation between the energy minimised and the registration technique is not formally established. Fig. 5 illustrates the deformations obtained when registering the 3D images of Fig. 1. It shows that the sliding motion we observed is captured when using sliding conditions. Quantitative results, shown in Table 1, allow to assess the benefit of using a diffeomorphic strategy with sliding conditions. Similar MI and deformation smoothnesses are obtained using all the techniques for the images requiring no sliding motion. Sliding conditions however improve the balance between matching quality (high MI) and

[1] www.doc.ic.ac.uk/∼dr/software/

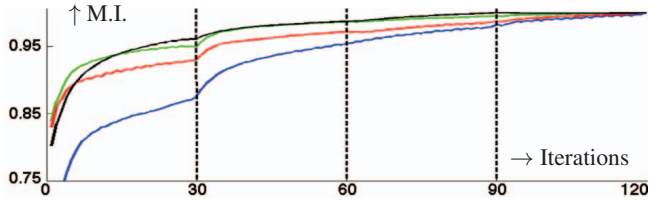


Fig. 4. Evolution of the Mutual information when registering four CT/MR scans with sliding motion. For each subject, the MI is normalised by its value after 120 iterations. Image resolution was increased at iterations 30, 60 and 90 respectively.

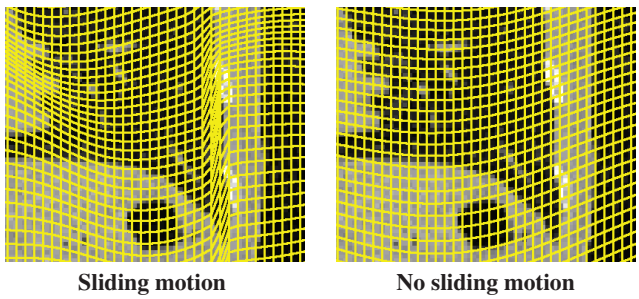


Fig. 5. Deformations estimated in the 3D CT/MR images of Fig. 1.

Table 1. Evaluation of the CT/MR registration using Log-Demons with **(PWLD)** or without **(LD)** sliding conditions and using free-form deformations **(FFD)** on the 12 most representative patients out of 14. Patients with stars (P. n*) present a sliding motion. **(M. Info.)** is the MI between the registered images. **(Std J)** is the standard deviation of the Jacobians in $\Omega - \partial\Omega_T$. **(Av)** and **(Av*)** are respectively the average values obtained for the 14 patients and on those presenting a sliding motion.

		P. 1	**P. 3**	**P. 4**	**P. 8**	**P. 10**	**P. 11**	**P. 14**	**P. 6***	**P. 7***	**P. 9***	**P. 12***	**P. 13***	**Av**	**Av***
M. Info.	**PWLD**	**0.37**	**0.65**	0.58	**0.50**	**0.57**	0.51	0.54	**0.42**	**0.51**	**0.52**	**0.49**	0.43	0.501	0.474
	LD	0.31	0.62	**0.60**	0.49	**0.57**	0.49	0.51	0.39	0.49	0.50	0.45	0.41	0.481	0.448
	FFD	**0.37**	0.44	0.59	0.46	0.56	**0.52**	**0.56**	**0.42**	0.50	0.51	**0.49**	**0.44**	0.485	0.472
Std J	**PWLD**	0.28	0.19	**0.30**	0.20	**0.22**	0.19	0.25	**0.29**	**0.24**	**0.18**	0.12	**0.17**	0.216	0.200
	LD	**0.17**	**0.09**	0.32	0.19	0.23	**0.17**	0.24	0.31	0.25	0.19	**0.10**	0.18	0.203	0.206
	FFD	0.57	0.31	0.57	**0.18**	0.38	0.30	**0.20**	0.38	0.30	0.24	0.19	0.30	0.317	0.282

deformation smoothness in $\Omega - \partial\Omega_T$ (low Std J) for the images presenting a sliding motion. The amount of negative Jacobians in our experiments was limited but non-null using FFD (0.147% voxels in average). No negative Jacobians were however obtained using the Log-Demon strategies. Note that registration accuracy measurement using landmarks was deemed not reliable due to the large slice thickness. Computational time was about 50 and 30 minutes[2] for the multi-modal Log-Demons registration with and without sliding motion modelling respectively, and several hours for the FFD.

4. CONCLUSION

We have presented a novel multi-modal diffeomorphic registration method which addresses the problem of sliding motion. The use of a diffeomorphic setting allows to model large deformations with locally strong discontinuities, whilst preserving mathematically the invertibility of the deformations. Sliding conditions also allowed us to incorporate a physiological information about the lung boundaries motion, leading to a more realistic registration within and around the lungs. This is particularly true in regions where the images contain few features and an advanced model is required to regularise the deformations. Future work will deal with further mathematical justification of the proposed model. More specifically, we will integrate the proposed piecewise-diffeomorphic registration strategy in the LDDMM formalism, where we will formalise the relation between the minimised energy and the optimisation strategy. Further tests of our method will also be performed on the MICCAI'10 Empire dataset [1]. We will also focus on modelling more finely the sliding conditions location. We finally expect that the proposed strategy should also be helpful for a wider range of applications where sliding conditions are needed, such as the liver or the heart.

5. REFERENCES

[1] K. Murphy, B. Van Ginneken, J. M. Reinhardt, S. Kabus, K. Ding, X. Deng, J. P. W. Pluim, and et. al, "Evaluation of registration methods on thoracic CT: The EMPIRE10 challenge," *IEEE Trans. Med. Imaging*, 2011.

[2] D. Ruan, S. Esedoglu, and J.A. Fessler, "Discriminative sliding preserving regularization in medical image registration," in *Proc. ISBI*, 2009, pp. 430 –433.

[3] A. Schmidt-Richberg, J. Ehrhardt, R. Werner, and H. Handels, "Slipping objects in image registration: improved motion field estimation with direction-dependent regularization," in *Proc. MICCAI*, 2009, pp. 755–762.

[4] Y. Yin, E. Hoffman, and C.-L. Lin, "Lung lobar slippage assessed with the aid of image registration," in *Proc. MICCAI*, 2010, vol. 6362, pp. 578–585.

[5] D. F. Pace, A. Enquobahrie, H. Yang, S. R. Aylward, and M. Niethammer, "Deformable image registration of sliding organs using anisotropic diffusive regularization," in *Proc. ISBI*, 2011, pp. 407 –413.

[6] T. J. Winkstern and N. D. Cahill, "Rapid DFT-based variational image registration with sliding boundary conditions," in *Proc. ISBI*, 2011, pp. 429 – 432.

[7] V. Delmon, S. Rit, R. Pinho, and D. Sarrut, "Direction dependent B-splines decomposition for the registration of sliding objects," in *Proc. MICCAI workshop PIA*, 2011, pp. 45 –55.

[8] L. Risser, H. Baluwala, and J. A. Schnabel, "Diffeomorphic registration with sliding conditions: Application to the registration of lung CT images," in *Proc. MICCAI workshop PIA*, 2011.

[9] T. Vercauteren, X. Pennec, A. Perchant, and N. Ayache, "Symmetric log-domain diffeomorphic registration: A demons-based approach," in *Proc. MICCAI*, 2008, pp. 754–761.

[10] M. Modat, T. Vercauteren, G. R. Ridgway, D. J. Hawkes, N. C. Fox, and S. Ourselin, "Diffeomorphic demons using normalized mutual information, evaluation on multimodal brain mr images," in *Proc. Med. Imag.*, 2010, p. 76232K.

[11] H. Lu, M. Reyes, A. Šerijović, S. Weber, Y. Sakurai, H. Yamagata, and Ph. C. Cattin, "Multi-modal diffeomorphic demons registration based on point-wise mutual information," in *Proc. ISBI*, 2010, pp. 372–375.

[12] L. Risser, M. P. Heinrich, D. Rueckert, and J. A. Schnabel, "Multi-modal diffeomorphic registration using mutual information: Application to the registration of CT and MR pulmonary images," in *Proc. MICCAI workshop PIA*, 2011.

[13] P. Thévenaz and M. Unser, "Optimization of mutual information for multiresolution image registration," *IEEE Trans. Imag. Proc.*, vol. 9, no. 12, pp. 2083–2099, 2000.

[14] W. P. Segars, *Development of a new dynamic NURBS-based cardiac-torso (NCAT) phantom*, Ph.D. thesis, UNC, 2001.

[15] D. Rueckert, L. I. Sonoda, C. Hayes, D. L. G. Hill, M. O. Leach, and D. J. Hawkes, "Nonrigid registration using free-form deformations: Application to breast MR images," *IEEE Trans. Med. Imaging*, vol. 18, no. 8, pp. 712–721, 1999.

[2] C++ language on an iMac with 2.93GHz Intel Core i7 and 8 GB memory